International Journal of Extreme Manufacturing

Morphological characteristics and atomic evolution behavior of nanojoints in Ag nanowire interconnect network

OPEN ACCESS
IOP Publishing | IMMT
International Journal of Extreme Manufacturing
Int. J. Extrem. Manuf. 5 (2023) 025503 (11pp)
https://doi.org/10.1088/2631-7990/acc434

Morphological characteristics and atomic evolution behavior of nanojoints in Ag nanowire interconnect network

Jianlei Cui[1,2,*], Xiaoying Ren[1], Xuesong Mei[1,2,*], Zhengjie Fan[1], Chenchen Huang[1], Zhijun Wang[2], Xiaofei Sun[1] and Wenjun Wang[1]

[1] State Key Laboratory for Manufacturing Systems Engineering, Xi'an Jiaotong University, Xi'an 710049, People's Republic of China
[2] State Key Laboratory of Solidification Processing, Northwestern Polytechnical University, Xi'an 710072, People's Republic of China

E-mail: cjlxjtu@mail.xjtu.edu.cn and xsmei@mail.xjtu.edu.cn

Received 16 November 2022, revised 15 January 2023
Accepted for publication 13 March 2023
Published 24 March 2023

Abstract

Ag nanowires (AgNWs) have shown great application value in the field of flexible electronics due to their excellent optical and electrical properties, and the quality of its joints of AgNWs in the thin film network directly plays a key role in its performance. In order to further improve the joint quality of AgNWs under thermal excitation, the thermal welding process and atomic evolution behavior of AgNWs were investigated through a combination of *in situ* experimental and molecular dynamics simulations. The influence of processing time, temperature, and stress distribution due to spatial arrangement on nanojoints was systematically explored. What is more, the failure mechanisms and their atomic interface behavior of the nanojoints were also investigated.

Supplementary material for this article is available online

Keywords: Ag nanowires, nanocontacts, morphological characteristics, atomic configuration, MD simulation

1. Introduction

The rapid development of flexible electronic devices has brought unprecedented changes to the world. Ag nanowires (AgNWs) are regarded as the most promising materials owing to their outstanding electrical, optical, and mechanical properties and the high-quality AgNW interconnection network is also widely used in the flexible electronics and transparent electrode industries. Nanojoining technology greatly enriches the preparation of functional nanostructures and nanodevices to improve the properties of AgNWs networks. Along with the rapid development of nanotechnology, nanojoining methods and mechanisms have become research hot spots [1–4]. To achieve high-quality joining of metallic nanomaterials, different nanojoining techniques have been used with various types of heat sources, including high-temperature annealing [5–7], Joule heat [8, 9], microwave sintering [10, 11], plasma sintering [12, 13], and high-energy beams (including electron beam [14, 15], ion beam [16–18] and laser beam [19–21]), etc. Regardless of the heat source, nanojoints are ultimately obtained. Direct high-temperature annealing has been widely used and investigated as an efficient method to fabricate large-scale interconnected networks of AgNWs. However, as the scale of the material shifts to the nanoscale, its thermal sensitivity increases significantly. High temperatures affect and

* Authors to whom any correspondence should be addressed.

2631-7990/23/025503+11$33.00

modify the structures of nanowires and nanojoints to a certain extent. Low-temperature joining is an important method for improving the quality and performance of nanojoints.

To reveal the dependence of nanojoint quality on temperature, in previous studies, the homogeneous interconnection behavior of nanowires containing various metals such as Au, Ag, and Cu under high-temperature treatment has also been studied, but the influencing factors affecting the quality of nanojoints in the AgNWs interconnect network are not only the temperature, and there are few analyzes on its atomic characteristics and welding mechanism. Therefore, to deeply understand and reveal the nanojoining mechanism and improve joints quality, this paper will investigate through a combination of *in situ* experimental and molecular dynamics (MD) simulations to directly reflect morphological characteristics and atomic evolution behavior of AgNW joints.

2. Materials and sample preparation

The AgNWs used in this study were purchased from Nanjing Xianfeng Nanomaterials Technology Co. Ltd. The morphology of the AgNWs is shown in figure 1. To compare the influence of the size of AgNWs on their welding characteristics, the morphology of AgNWs used in this study had two specifications. One of the AgNWs had an average diameter of approximately 30–40 nm and a length of 20–30 μm with the diffraction spot showing a single-crystal nanowire with a crystal orientation [110]. The other had an average diameter of 120–150 nm and a length of 60–70 μm. Although it also grew along the [110] crystallographic direction, there were nanoparticles on the surface, and the diffraction spot was elongated, showing the existence of some twinning structures. The surface of the nanowires was a [111] plane, and the interplanar spacing was approximately 0.235 nm. Both nanowires had a protective layer of polyvinylpyrrolidone (PVP) with a thickness of approximately 2 nm, which was left over from the synthesis process. The heating process was mainly carried out in a vacuum tube furnace (heating range: room temperature to 1100 °C), and the morphology and atomic interfaces were observed conducting scanning electron microscopy (SEM) and transmission electron microscopy (TEM).

To investigate the morphological characteristics of AgNWs during thermal induction, the wires were spin-coated and dispersed on a clean silicon substrate, and then heated in vacuum tube furnaces. Morphological changes were observed at various temperatures and times. Each sample at different temperatures and times was stored at 25 °C for 1 d in a vacuum oven to eliminate the effects of residual temperature and stress, as well as the effects of atmospheric environmental elements.

3. Experimental results and discussion

3.1. Surface and interface characteristics of AgNWs after nanojoining

The experimental results show that for the heating-induced welding method, the final quality of the joint has a strong sensitive relationship with the initial spacing and orientation of the arrangement between nanowires. Three types of nanojoints can be obtained during the welding process: head-to-head, head-to-side (T-type), and side-to-side (X-type) joints. As shown in figure 2, it is a schematic diagram of three arrangements of nanowires to be welded. These three types are divided into two major categories based on their spatial structure characteristics, for head-to-head joints and T-joints, since the arrangement of these two joints belongs to the same horizontal plane, there is no relative positional relationship between the upper and lower spaces, the main influence on its welding characteristics is due to their spacing 'D' in the horizontal plane. For X-shaped nanojoints, because of their upper and lower spatial structure characteristics, the distance has little influence on them, and their joint morphology is mainly influenced by stress concentration during the welding process as well as the inhomogeneity of the electrostatic force existing between the nanowires and the substrate under different configurations. Moreover, under thermal excitation, the X-joint may have fluid-like capillary features in the vertical pores.

In theory, head-to-head joints are easier to achieve because they have a higher surface energy at both ends, and more defects overhang the ends to aid atomic diffusion. Although the more the overhanging atomic vacancies on the interconnection surface, the easier the interconnection. However, X-shaped joints are the easiest to achieve in practice. This is because this form of nanowire ensures close contact spacing at the intersection, allowing for interdiffusion at lower temperatures, and the local stresses at the nanojoint may also assist the welding process. The head-to-head nanojoints are separated by a certain distance and fused at the gap by heating and expanding the diffusion flow. The T-junctions are the most difficult to obtain. Compared to the head surface, the side surface of the nanowire needs more energy to be destroyed, and the spacing between the nanowires also needs to be sufficiently close.

For AgNWs with a diameter of 30 nm, heated and treated at 150 °C for 30 min, a good interconnection mesh could be achieved, and no excessive morphological damage is produced in the non-junction region, as shown in figures 3(a)–(c). As shown in figures 3(d)–(f), the interfacial atomic morphologies of the different types of joints exhibit different atomic behaviors. Figure 3(d) shows the interfacial characteristics of the head-to-head nanowires after 30 min of treatment at 150 °C. It can be seen that for the head-to-head form of the nanowire joints, there are a large number of twin structures at the interface, and there is a tendency for the two sets of crystal orientations of the nanowires to converge as the welding process proceeds. Although the PVP layer at the head of the nanowire induced corresponding amorphous defects at the joint, the defects gradually moved to the edge of the joint with the active movement of the head atoms, and the overall nanojoining process was less affected by the PVP layer. Figure 3(e) shows the interfacial characteristics of the T-joint after 30 min of treatment at 150 °C. The results show that the T-joint has more interfacial defects and a greater number of amorphous structures compared to the head-to-head joint form because the PVP layer on the surface of the nanowire

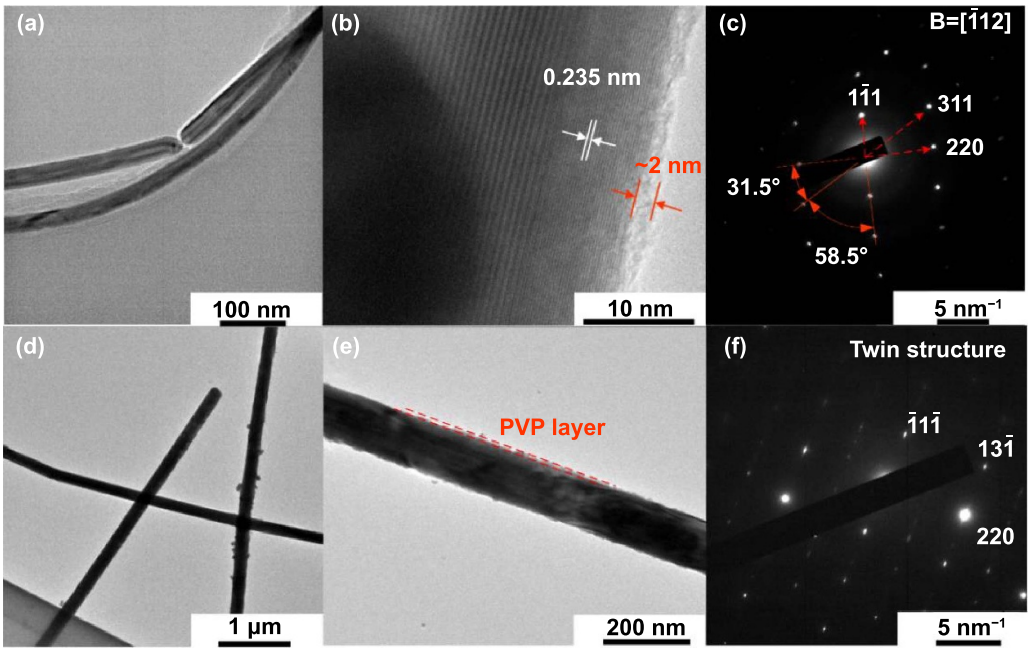

Figure 1. Initial morphology and atomic distribution characteristics of AgNWs with different sizes. (a)–(c) Diameter of approximately 30–40 nm; (d)–(f) diameter of approximately 120–150 nm.

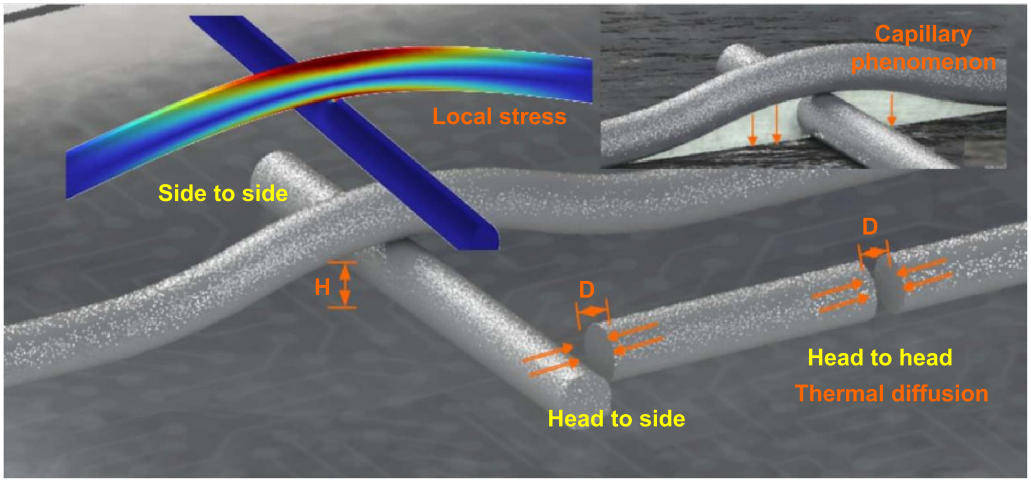

Figure 2. Schematic diagram of three spatial arrangements of Ag nanowires.

side body cannot be extended along the joint to both sides of the joint, just like in the case of the head-to-head form of the joint. Although a residual layer of PVP can be discharged at the end of the nanowire, some of it remains inside the welded joint and causes certain defects. The diffusion process of this type of joint is more inclined to the diffusion of the head atoms in the T-joint to the vertical nanowire axis body, whereas some nanoparticles are excited during the heat transfer process, accompanied by the excitation and fusion of Ag nanoparticles to achieve the complete fusion of the T-joint. As for the X-type joints, because the PVP layers of both AgNWs to be welded cannot be avoided by atomic motion during the welding process, the PVP layers on both sides are preferentially cross-linked owing to the interference of the PVP layers. As the nanojoining process proceeds, the activity of Ag atoms intensifies. Some of the excited nanoparticles break through the PVP layers, and a large number of nanoparticles encapsulated with PVP are generated and diffuse into the gap of the nanowire to facilitate the subsequent welding process, as shown in figure 3(f). Most of these small-sized nanoparticles are face-centered cubic (FCC) single-crystal structures; however, their surfaces are wrapped with a thick amorphous carbon layer, resulting in a large number of defects at the joints. For AgNWs with a diameter of 100–150 nm, the heating temperature needs to reach 200 °C to obtain good nanojoints, as shown in figures 3(h)–(j). Moreover, compared to smaller nanowires, the surface of AgNWs with a diameter of 100–150 nm is more likely to form bumpy nanostructures during the welding process, as shown in figures 3(g) and (h). These nanostructures are consistent with the function of nanoparticles to act as a solder

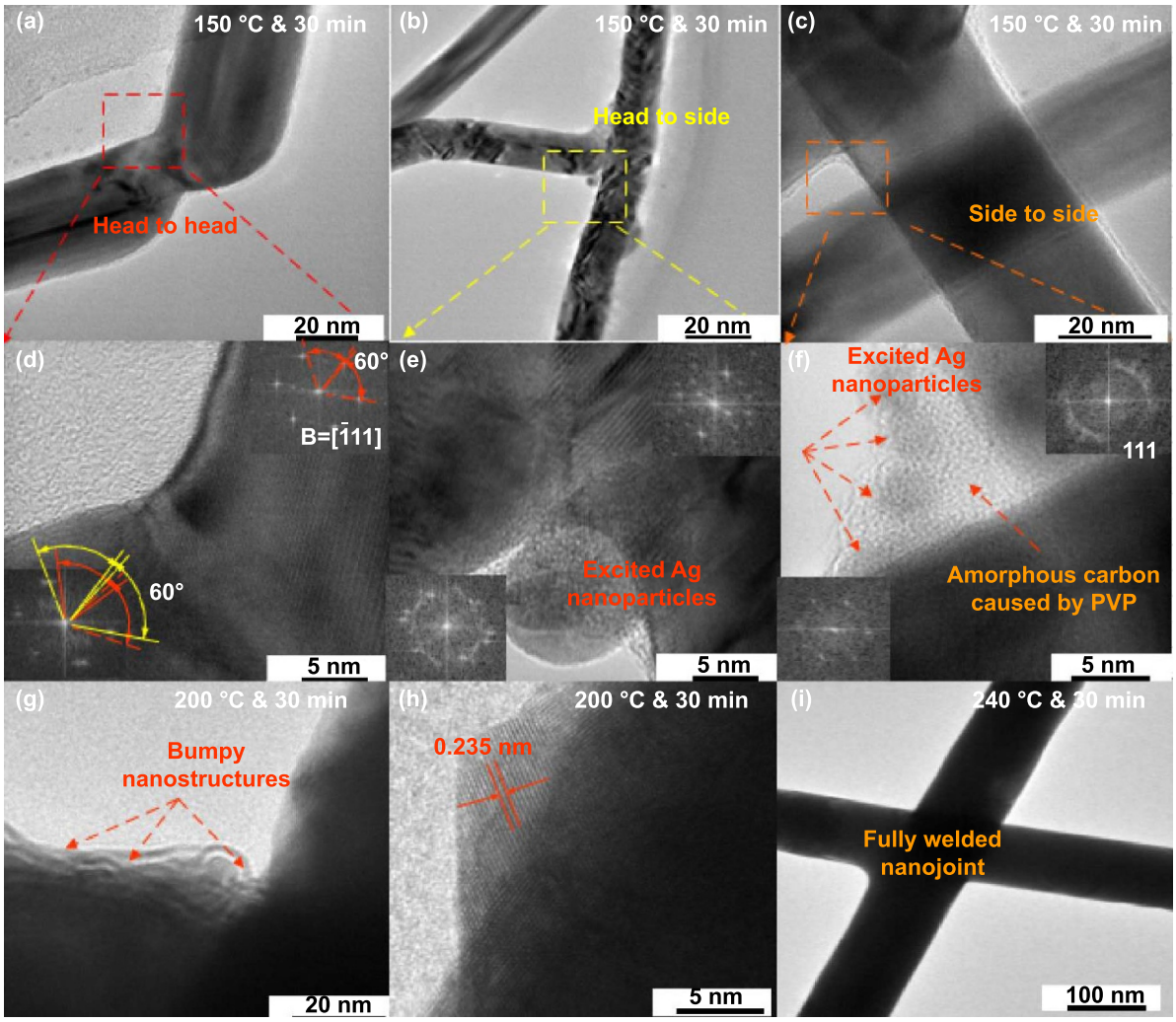

Figure 3. Interface and atomic distribution characteristics of nanojoints with different sizes. (a)–(f) Morphology of AgNWs with diameter of approximately 30–40 nm treated at 150 °C for 30 min; (g)–(i) morphology of AgNWs with diameter of approximately 100–150 nm treated at 200 °C for 30 min.

to facilitate complete soldering between nanowires. Eventually, as the soldering process proceeds, the top and bottom crossed nanowires gradually spread to a plane, forming a distinct necked joint, as shown in figure 3(i).

In addition, because of the spatial distribution characteristics of the X-type joint, it had significantly different characteristics than the other two joints in the welding process. To further analyze the characteristics of the connection process, besides top morphology, we also studied the welding-side morphology of the X-joint. It can be seen from the experimental results that for nanowires with large diameters and high aspect ratios, a large number of hole structures are formed in the vertical direction between the intersecting nanowires. However, when a higher temperature is applied, with the accelerated flow of atoms on the surface of the nanowire, these hollow structures gradually become close to the surface. Thus, a relatively obvious concave–convex structure will be formed at both ends of the X-joint, causing the atoms of the upper nanowire to accelerate to the bottom, and gradually wrap the nanowires in the lower layer, as shown in figure 4. At the same time, with an increase in the welding process, at the gap between the nanowire and the substrate, the surface of the nanowire generates uneven surface flow owing to the temperature gradient, at a certain temperature, as the welding time increased, the nanowires in the lower layer gradually became embedded in those in the upper layer. Under the influence of capillary, electrostatic force, and temperature gradient, mutual diffusion between atoms is accelerated to form stable nanojoints.

3.2. Behavior and welding mechanism of AgNWs under thermal excitation

In order to further explain the welding mechanism of AgNWs under thermal excitation, we carried out *in situ* heating experiments in SEM and TEM systems. As mentioned earlier, AgNWs will be accompanied by a large number of Ag nanoparticles during thermal excitation, firstly we analyzed the microscopic morphology evolution characteristics of AgNWs under thermal excitation through SEM *in situ*

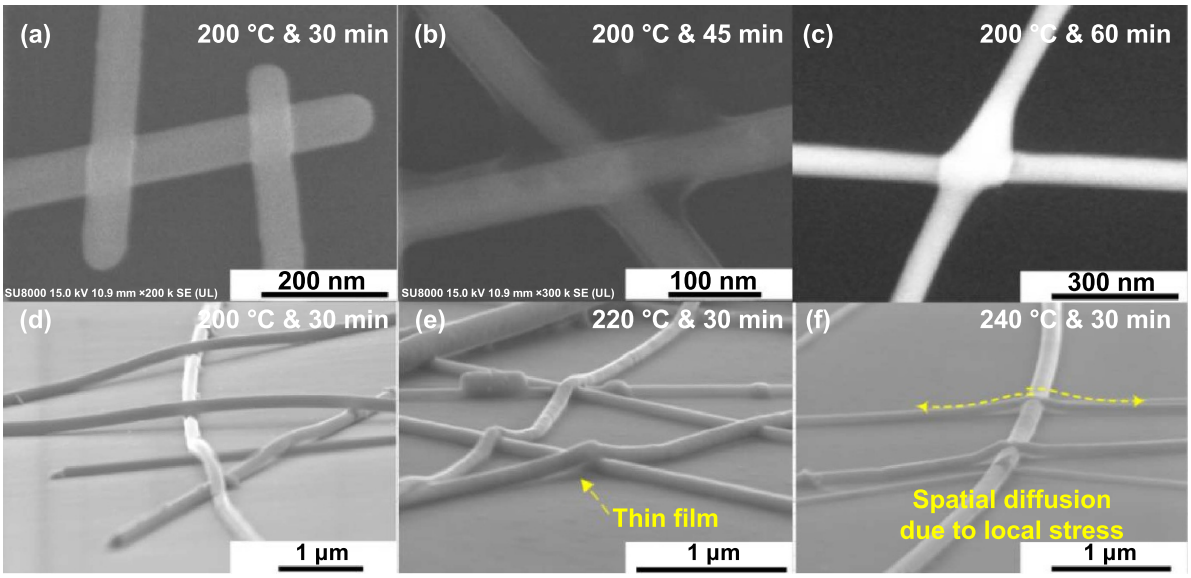

Figure 4. Morphological characteristics of X-joints. (a)–(c) Diameters of 30–50 nm treated at 200 °C for 30, 45, and 60 min; (d)–(f) diameters of 100–150 nm from 70° viewing angle.

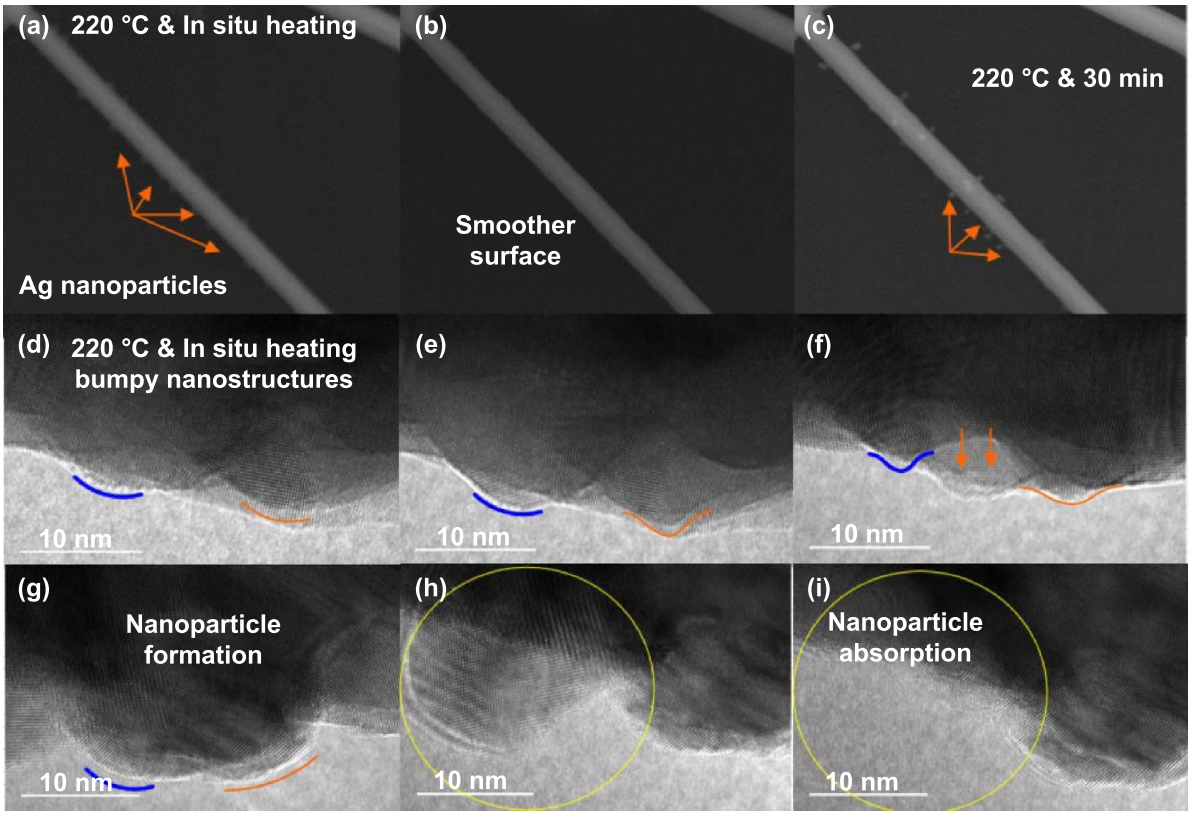

Figure 5. Morphological evolution of nanoparticles on the surface of Ag nanowires. (a)–(c) *In situ* heating in SEM; (g)–(h) *in situ* heating in TEM systems.

heating experiments, just shown in figures 4(c) and 5(a), we can observe that when the nanoparticles remaining on the surface of AgNWs are heated, driven by the surface energy, the surface of the nanowires will become smooth at first, but with the heating process, the surface of the AgNWs will re-excite a large number of nanoparticles. The mechanism of the formation of nanoparticles may be due to Capillary-induced surface diffusion and penetration. As shown in figures 4(i) and 5(d), we conducted *in-situ* heating experiments in the TEM system, and the results clearly show the atomic lattice evolution process of the AgNW interface under thermal excitation. The evolution process video can also be found in movie

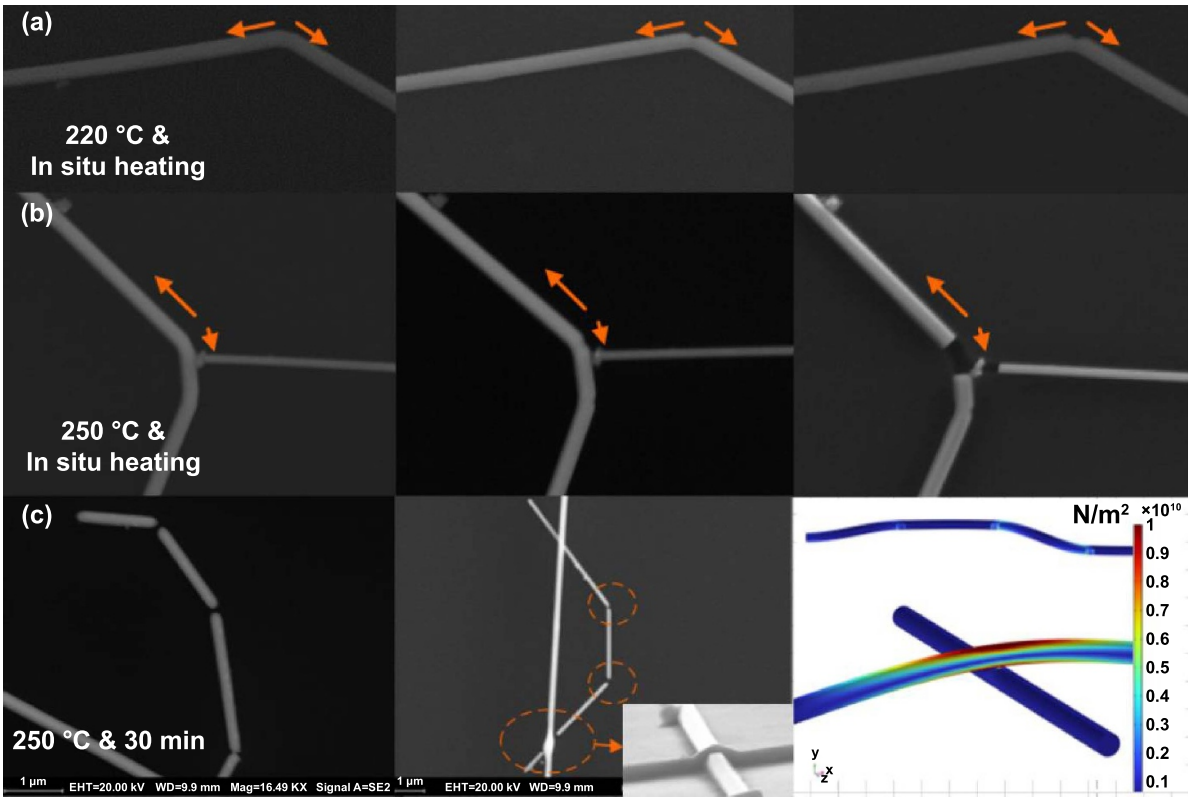

Figure 6. The stress-driven morphology characteristics of Ag nanowires under thermal excitation. (a) The morphology evolution of Ag nanowires under *in-situ* heating at 220 °C; (b) the morphology evolution of Ag nanowires under *in-situ* heating at 250 °C; (c) morphological characteristics of the Ag nanowires at the curvature part and the cross junction after the Ag nanowires were heated at 250 °C for 30 min.

1 in the supporting file. At the interface of the nanowires, accompanied by the thermal motion of the atoms under the capillary, local raised nanostructures are induced, and the Ag atoms in these structures will be reoriented under the drive of the surface energy, interdiffusion between adjacent nanostructures gradually forms single-crystal nanoparticles. When these nanoparticles are aligned with the AgNWs, they will be reabsorbed and rearranged. Therefore, when two nanowires are being welded, the surface atoms of the nanowires are rearranged and fused together to obtain a welded joint, this is why as the heat treatment time increases, the crystal plane defects at the joint will become less and less. As the temperature increases, the sputtering process of nanoparticles will become more and more intense.

In addition, as mentioned in the first part, for AgNWs, especially for crossed nanojunctions, the welding morphology will be greatly affected by local stress. In order to further study welding diffusion mechanism of stress on AgNWs, we performed *in situ* heating experiments just shown in figure 6, we found that AgNWs will have a certain stress concentration in the parts with curvature, these parts often show localized damage or fracture under thermal excitation. At the same time, for crossed nanowires, it often shows the characteristic that the upper nanowires flow to both sides of the bottom nanowires. What is more, simulation results show that the maximum strain of the upper nanowires is about 0.5%, it is in the elastic stage and will flow to both sides of the joint under the drive of local stress. For AgNWs with a certain aspect ratio, when the strain at the curvature position exceeds the elastic strain range, there will be a certain plastic deformation. More detailed simulation information can be found in supporting document.

3.3. Influence of temperature and time on behavior and characteristics of AgNWs during nanojoining

More importantly, as mentioned earlier, for AgNWs with diameters between 30 and 40 nm, good joints were obtained after 30 min at 150 °C, whereas for T- and X-type nanojoints, higher energies were required to facilitate the welding process because of the difference in atomic surface energies at the contact surface, as shown in figures 7(a)–(c). It was also found that at the same processing time, with an increase in the processing temperature of the sample, the flow of the nanowire will be accelerated, and the interconnection interface became more sufficient. The suitable interconnection temperature for nanowires with diameters of 30–40 nm was 150 °C–190 °C, and for nanowires with diameters 100–150 nm, the suitable interconnection temperature was 200 °C–240 °C, more detailed welding morphology can be found in supporting files. The temperature difference may be due to the size effect and the change in thermal conductivity with size. The results shows that with an increase in the welding temperature, the size of the head of the nanowire gradually increases owing to the axial flow of atoms, as shown in figure 7(a), the T joint and X joint are also welded more and more fully, especially for the X-joint at this time, under the influence of

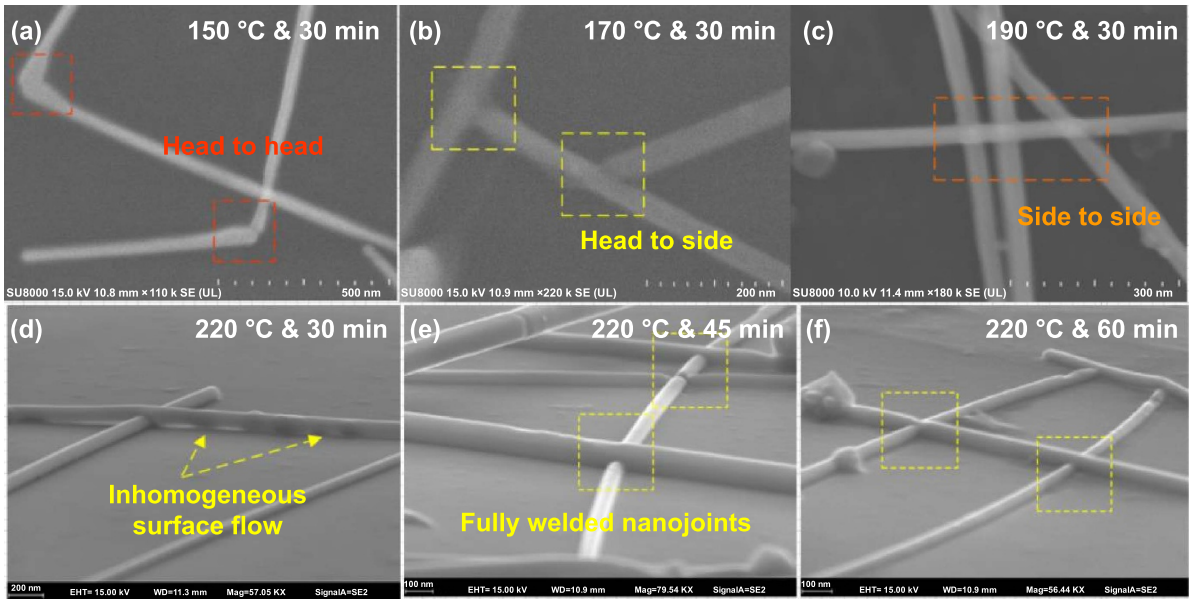

Figure 7. Microscopic morphological characteristics of AgNWs treated at different temperatures and times. (a)–(c) Microscopic morphological characteristics of AgNWs with diameters of 30–50 nm treated for 30 min at 150 °C, 170 °C, and 190 °C; (d)–(f) morphological characteristics of AgNWs treated for different times.

thermal excitation and capillary, the nanowires will accelerate to the bottom. Furthermore, there may be some unstable spatial structures that form high local stresses after cooling.

In addition, to study the effect of time on the morphological characteristics of the joint at the same temperature, with an increase in welding time, the atomic diffusion of nanowires tends to be more stable, as shown in figures 8(d)–(f). For the X joint, as time increases, the holes in the vertical direction are gradually filled, and the most stable joints are achieved. Therefore, increasing the processing time at low temperatures is more conducive to the formation of stable interconnected networks than increasing the temperature, which may lead to the final formation of unstable structures.

For AgNWs with diameters of 30–50 nm, when the heat treatment temperature exceeded 200 °C, the three joints exhibited large morphological changes, and certain thermal damage and fracture occurred successively. When the samples were treated at 200 °C for 30 min, the T-type joints diffused sufficiently, and the joint morphology exhibits ductile flow along the axial direction of the nanowires, as shown in figure 8(a). The results showed that the nanojoining became increasingly adequate, and the ductility tended to increase with time. However, for the other two types of joints, the nanowires were subjected to an increased region of thermal influence. The nanowires increased in diameter owing to a tendency to shrink axially, and weak zones begin to appear on both sides of the upper nanowires in X-type joints, as shown in figures 8(b) and (c). As the temperature continued to increase, we could clearly see that some parts of the nanowire started to show obvious damage, and its surface was surrounded by densely ablated nanoparticles. With a further increase in temperature, a part of the X-joint on both sides of the joint begin to fracture, as shown in figure 8(e), the nanoparticles produced on the surface were partially reabsorbed and fused, and then partially split into smaller particles. For AgNWs with diameters of 150–200 nm, the aspect ratio was longer. When the soldering temperature exceeds 260 °C, as the temperature continues to increase, it exhibits similar characteristics as small-sized nanowires, with defects and fractures occurring on both sides of the X-type joint. As the temperature continues to increase, the atoms are more inclined to continue to flow along the axial direction, condensing into large particles at the defect site, and are not more likely to form nanoparticle arrays due to Rayleigh instability, just like small-sized nanowires, as shown in figure 8(f).

To further analyze the damage mechanism of the joint under thermal disturbance, we made further observations of its atomic behavior. In the process of X-joint formation, the upper nanowires flow violently under the influence of high temperatures and flow along the lower nanowires, resulting in the most violent flow of nanowires and the weakest flow on both sides of the joint. Compared to the first two types of joints, this joint type has the most defects and is the most prone to later damages owing to thermal disturbances. At a welding temperature of 210 °C, when the broken AgNWs at the X-joint begin to show obvious axial shrinkage with the increase in time, and the spacing becomes increasingly farther, joint fracture is more likely to occur under thermal disturbance at the X-joint. One possible reason is that the X-joint itself has many defects, and its local thermal stress reaches a high value. Under thermal perturbation at a certain temperature, the nanowire first thermally fractured on both sides of the X-joint of the upper nanowire owing to the Rayleigh instability of the nanowire surface and the local stress of the joint. At the same time, with a further increase in temperature, the nanowires were completely disrupted and ablated into isolated nanoparticles, which showed a tendency to polycrystallize, and the residual PVP layer encapsulated some small particles

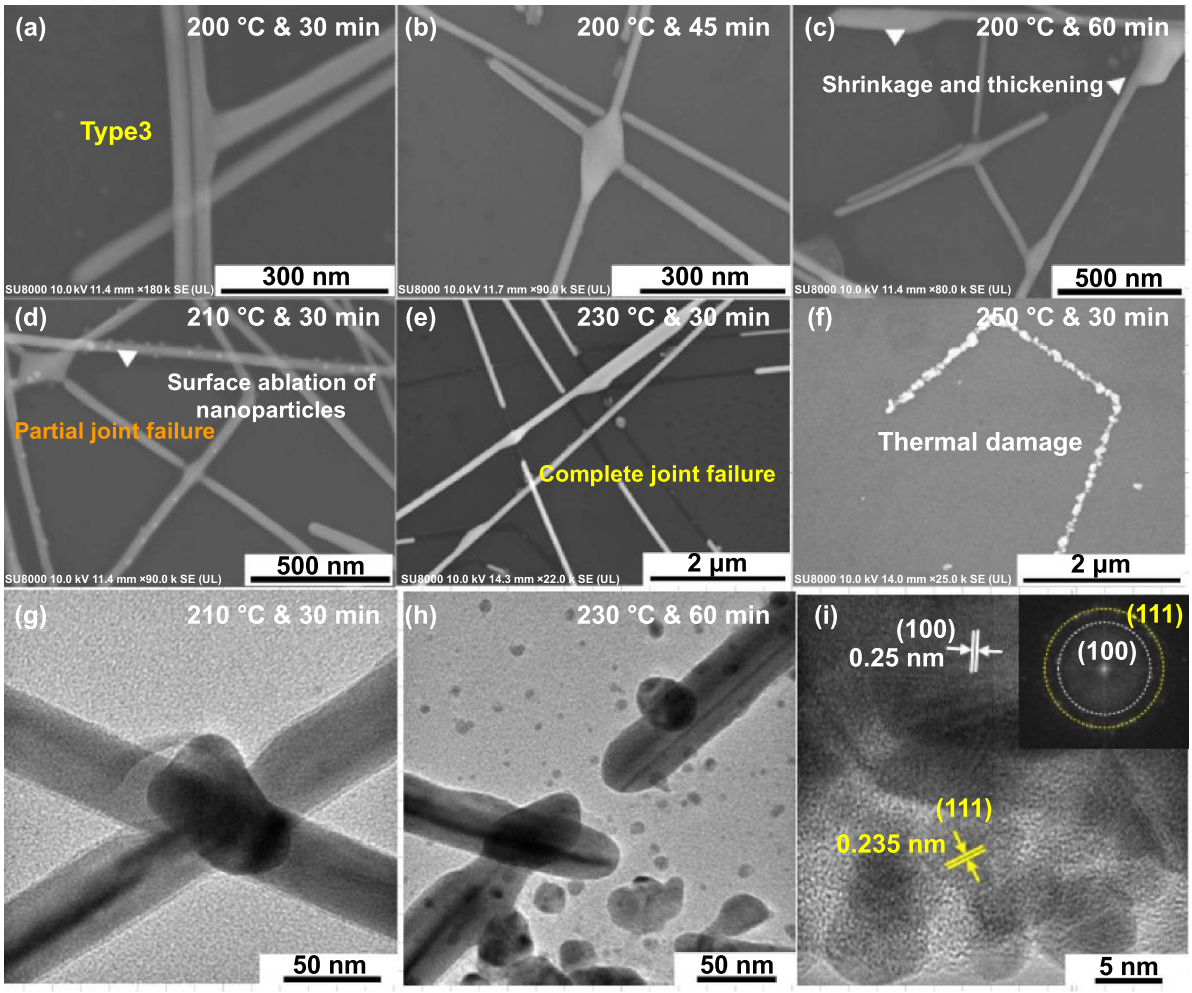

Figure 8. Atomic morphology of AgNWs treated at different temperatures and times. (a)–(c) Morphological characteristics of AgNWs with diameters of 30–50 nm at 200 °C for 30, 45, and 60 min; (d)–(f) morphological characteristics of AgNWs with diameters of 30–50 nm treated for 30 min at 210 °C, 230 °C, and 250 °C; (g)–(i) atomic interface characteristics of X-type nanojoints.

and prevented further fusion, as shown in figures 8(g)–(i). However, as the heating time increased, the fusion between the particles become more sufficient, the shape of the broken particles became increasingly uniform, and finally, spherical particles were formed. For the T-type and head-to-head planar joints, because there was no space for flow, as the temperature increased, the axial shrinkage of the nanowires intensified and some large nanoparticles began to split at the welding position. These nanoparticles have some twinning interfaces, whereas some amorphous structures remain at the junctions affected by the residual PVP layer, more detailed TEM can be found in supporting documents.

4. Simulation results and discussion

4.1. Atomic behavior and configurations during nanojoining of AgNWs

To better analyze the joint morphology and characteristics of AgNWs during the nanojoining process at the atomic scale, the atomic behavior of AgNWs during the thermally induced process was simulated using the MD. The initial model atoms were arranged in a standard FCC structure, and the AgNW lattice constant was set to 0.409 nm. Embedded atomic potential was used to study the joining process. To achieve a steady state, the energy of the entire system was minimized so that all atoms reached equilibrium, thus naturally introducing some lattice defects and bringing the simulated structure closer to reality. The diameter of each nanowire in the model was approximately 3 nm, the length was approximately 30 nm, and the time step was chosen to be 0.005 ps. First, relaxation was performed at 300 K for 40 ps, after which the temperature of the system was increased from 300 K to 450 K. This process lasted for 40 ps, and then a constant temperature was maintained at 450 K for 40 ps, after which the system was cooled from 450 K to 300 K.

First, we simulated the morphological characteristics of the head-to-head nanowire welding process. During the previous experiments, we found that the head-to-head form of nanojoints, owing to their higher surface activity, will get close to each other under a certain spacing owing to electrostatic force, and thus, achieve contact diffusion to obtain nanojoints.

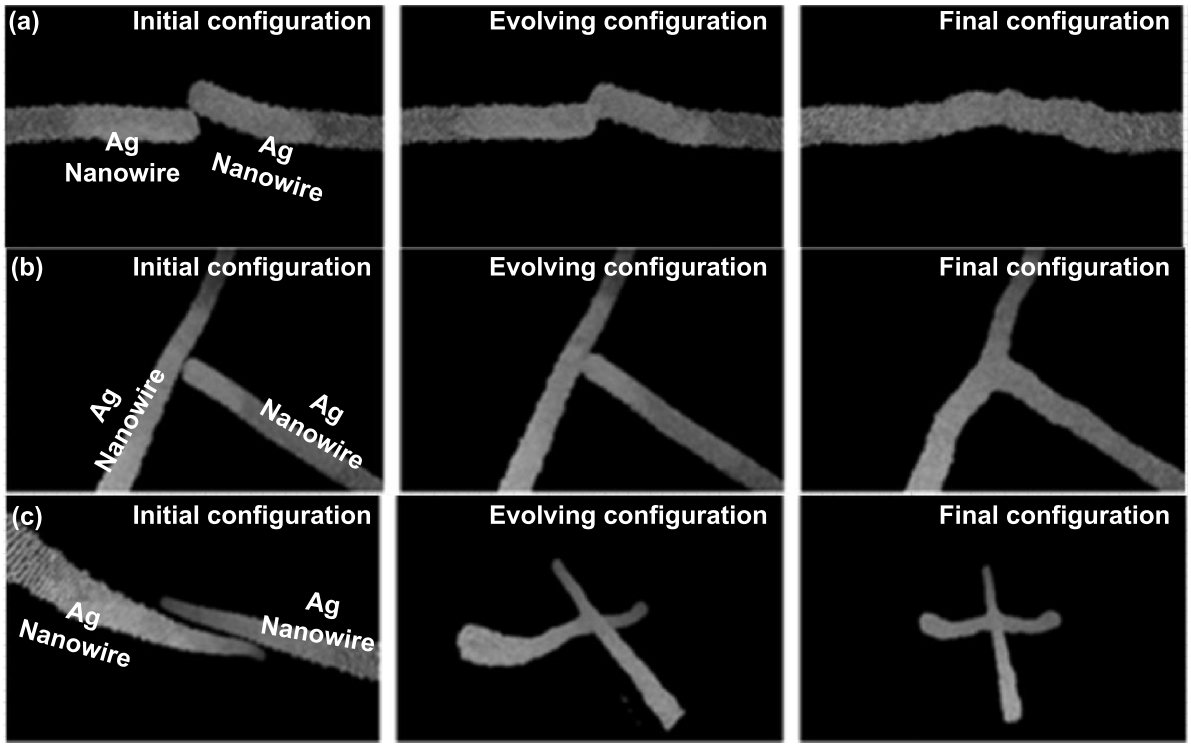

Figure 9. Atomic evolution behavior during welding process of (a) head to head; (b) T- and (c) X-joints of AgNWs.

However, when the separation spacing was beyond the range of the electrostatic force, or when the electrostatic force could not overcome the friction between the substrate and the nanowires, the spatial arrangement between the nanowires had a significant influence on the final joint morphology. To study the effect of distance on the joint morphology during the welding process, we set the nanowires to be welded at the same temperature and different spacing arrangements. When the initial distribution of the nanowires to be welded has a certain distance beyond the range of the electrostatic force, with the radial expansion and axial contraction of the AgNWs, along with the heat accumulation process, the distance between the two nanowires increases further, making it impossible to obtain a joint for head-to-head interconnection, as shown in supporting document and video 4. When the nanowire spacing is set within the interaction between atoms, as shown in figure 8(a), head-to-head nanowire joints can be more easily obtained owing to the accompanying radial thermal perturbation and expansion under the same heat-treatment conditions. The joints became fully welded over time.

For analysis of the X- and T-joints in figures 9(b) and (c), at the same temperature setting, the T-joints were welded together with the diffusion of AgNWs in the radial direction. The joint size becomes increasingly obvious with the increase in the joining process, and it can be seen that the atoms in other parts of the nanowires diffuse towards the joint during the nanojoining process. The atoms at the joint increasingly diffuse completely, and the size of the weld neck becomes increasingly larger, which is consistent with that in the experiment. For the X-shaped nanojoint, at the same temperature setting, the two nanowires were gradually welded together as they diffused radially. However, as the welding process proceeded, the upper nanowire atoms gradually diffused into the lower layer. This resulted in a decrease in the thickness of the nanojoint and the presence of more defects and disordered structures in this region, causing thermal stress and weakening of the properties of this part compared to the other parts. Similarly, the atoms at both ends of the nanowires were accompanied by inward shrinkage along the axial direction.

4.2. Comparative study of MD and experiment on atomic evolution behavior and configuration during the nanojoining of AgNWs

To investigate the damage and rupture behavior of Ag nanojoints in the experiments shown in figure 3, the factors influencing the thermal failure of single AgNWs under the action of different temperatures and times were first analyzed. It was found experimentally that the nanowires were often accompanied by axial shrinkage and radial ductility during the joining process; nanowires with a large aspect ratio (length of 160 nm and diameter of 3 nm) were constructed for heating simulations to better investigate the damage and rupture phenomenon of AgNWs. The model system was first stabilized by energy minimization and a low-temperature relaxation process, followed by a phased ramp-up from 300 K to 500 K under the NVT system. The simulation results in figure 9 show that as the temperature increases, the AgNWs begin to slowly contract axially and produce wave nodes in the radial direction owing to the Rayleigh instability of AgNWs

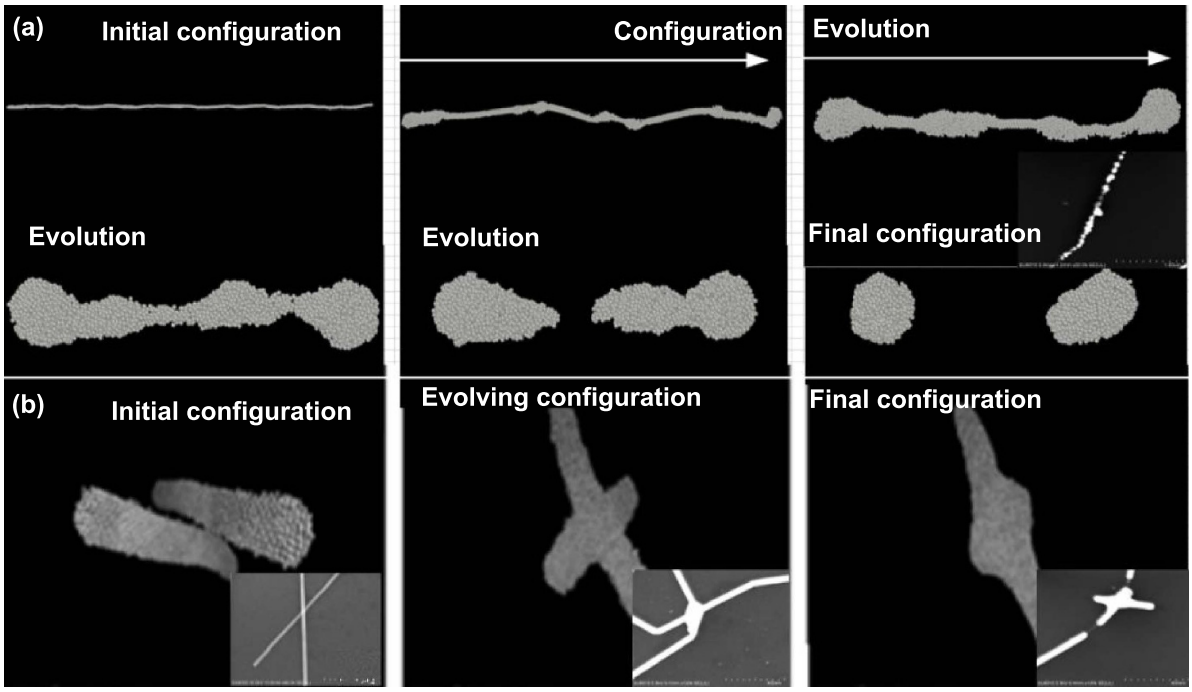

Figure 10. Morphological characteristics and atomic evolution behaviour of AgNWs nano-joints under thermal induction. (a) Thermal instability of AgNWs under thermal excitation; (b) atomic evolution behavior of X-joint at 500 K.

with fluid-like characteristics under thermal excitation, and sputtered nanoparticles appear. Moreover, as the temperature continued to increase, the number of particle-like joints increased and gradually stabilized, while these irregular Ag nanoparticles gradually split to form separate nanoparticles as the heating time continued to increase, the results are shown in figure 10(a), more detailed evolution process can be found in supporting document videos 5 and 6.

In case of the thermal damage of nanojoints, it is known from previous experimental results that X-joints, although the easiest to obtain, are the most likely to fail first, followed by head-to-head and finally T-joints. This is because Rayleigh instability occurs on the nanowire surface under the influence of high temperatures and is often accompanied by axial shrinkage and radial diffusion. When T- and head-to-head joints are obtained, both are spatially in the same plane and suffer much less thermal stress under thermal excitation than X-joints, while the proportion of disordered structures in the joints is relatively high because of the spatial diffusion of atoms up and down in the X-joints. Therefore, in this study, we modeled the atomic evolution process of X-type joints on an atomic scale. To develop the initial model for studying the welding mechanism, two AgNWs with a diameter of approximately 3 nm and a length of approximately 40 nm were constructed using the same temperature and initial settings as described above for the single failure temperature setting. The results are shown in figure 10(b), more detailed evolution process can be found in supporting document video 6. As the nanojoining process proceeded, the upper AgNW atoms diffused much faster than the lower atoms, and their axial shrinkage became more severe. The atoms on the upper nanowire diffused rapidly into the joint region and outwards along the lower nanowire, whereas the lower atoms, although with partial shrinkage, had a less pronounced shrinkage effect and mainly increased in the radial direction. Owing to their increased disordered structure at the joints, the local Rayleigh instability of the nanowires was already caused to appear at a lower processing temperature than that of the individual nanowires. This was accompanied by the continued formation of a large number of defective structures at the joints, with the upper nanowires being the first to fracture and fail at the ends of the joints as the heating process progressed, which is similar to previous experimental results.

5. Conclusions

In this paper, through the analysis of the welding process of AgNWs with different diameters, the influencing factors and characteristics of the three joint types of head-to-head, T-joint, and X-joint in the welding process are systematically discussed from the perspective of experiment and simulation, and the atomic interface behavior are also analyzed. More importantly, through the combination of *in situ* SEM and TEM experiments, the evolution and mechanism of the welding process of AgNWs under thermal excitation are deeply revealed, the thermal defect characteristics of the joints owing to the Rayleigh instability and local stress during the high-temperature process are also discussed. For AgNWs with a diameter of 30–40 nm, the experimental results show that the suitable welding process temperature is between 150 °C and 200 °C, whereas for AgNWs with a diameter of 100–150 nm, the results show that the suitable soldering process temperature

is between 200 °C and 240 °C. In this temperature range, with an increase in processing time, the atomic flow of the joint becomes increasingly sufficient, and the quality of the joint increasingly improves. In the welding process of AgNWs, in addition to being affected by temperature and time, the spatial distribution structure of AgNWs also has a significant influence on the quality of their joints. Compared to flat joints such as head-to-head and T-joints, the X-joint has upper and lower space positions during the welding process, therefore, it is more likely to be affected by the unbalanced stress between the various parts during the welding process, thereby introducing more defects at the joint. What's more, the upper nanowires will quickly diffuse to the bottom and wrap the bottom nanowires, nanofilms are formed inside these vertical hollow structures, which promotes the formation of a more stable structure of the nanojoint. The study of these features can provide support for facilitating the fabrication of AgNW interconnection networks and their further large-scale micro-nano device applications.

Acknowledgments

This work is supported by National Natural Science Foundation of China (Grant Nos. 52022078 and 51875450), Shaanxi Provincial Key Research and Development Program (Grant No. 2021ZDLGY10-02), the fund of the State Key Laboratory of Solidification Processing in NPU, (Grant No. SKLSP202203).

ORCID iDs

Jianlei Cui https://orcid.org/0000-0002-5760-509X
Xiaofei Sun https://orcid.org/0000-0001-7026-4317

References

[1] Zhou Y and Hu A 2010 From microjoining to nanojoining *Open Surf. Sci. J.* **3** 32–41
[2] Peng P, Hu A M, Gerlich A P, Zou G S, Liu L and Zhou Y N 2015 Joining of silver nanomaterials at low temperatures: processes, properties, and applications *ACS Appl. Mater. Interfaces* **7** 12597–618
[3] Xiao M, Zheng S, Shen D Z, Duley W W and Zhou Y N 2020 Laser-induced joining of nanoscale materials: processing, properties, and applications *Nano Today* **35** 100959
[4] Karthikeyan A and Mallick P S 2017 Optimization techniques for CNT based VLSI Interconnects-a review *J. Circuits Syst. Comput.* **26** 1730002
[5] Lu Y, Huang J Y, Wang C, Sun S H and Lou J 2010 Cold welding of ultrathin gold nanowires *Nat. Nanotechnol.* **5** 218–24
[6] Ding M N, Sorescu D C, Kotchey G P and Star A 2012 Welding of gold nanoparticles on graphitic templates for chemical sensing *J. Am. Chem. Soc.* **134** 3472–9
[7] Celano T A, Hill D J, Zhang X, Pinion C W, Christesen J D, Flynn C J, McBride J R and Cahoon J F 2016 Capillarity-driven welding of semiconductor nanowires for crystalline and electrically ohmic junctions *Nano Lett.* **16** 5241–6
[8] Tohmyoh H and Fukui S 2009 Self-completed Joule heat welding of ultrathin Pt wires *Phys. Rev.* B **80** 155403
[9] Raj R 2012 Joule heating during flash-sintering *J. Eur. Ceram. Soc.* **32** 2293–301
[10] Xie X *et al* 2014 Microwave purification of large-area horizontally aligned arrays of single-walled carbon nanotubes *Nat. Commun.* **5** 5332
[11] Gunnewiek R F K, Perdomo C P F, Cancellieri I C, Cardoso A L F and Kiminami R H G A 2020 Microwave sintering of a nanostructured low-level additive ZnO-based varistor *Ceram. Int.* **46** 15044–53
[12] Wang R R, Zhai H T, Wang T, Wang X, Cheng Y, Shi L J and Sun J 2016 Plasma-induced nanowelding of a copper nanowire network and its application in transparent electrodes and stretchable conductors *Nano Res.* **9** 2138–48
[13] Liu J F, Ge Y J, Zhang D M, Han M, Li M X, Zhang M, Duan X D, Yang Z L and Hu J W 2021 Plasma cleaning and self-limited welding of silver nanowire films for flexible transparent conductors *ACS Appl. Nano Mater.* **4** 1664–71
[14] Banhart F 2001 The formation of a connection between carbon nanotubes in an electron beam *Nano Lett.* **1** 329–32
[15] Terrones M, Banhart F, Grobert N, Charlier J C, Terrones H and Ajayan P M 2002 Molecular junctions by joining single-walled carbon nanotubes *Phys. Rev. Lett.* **89** 075505
[16] Wang Z X *et al* 2004 Amorphous molecular junctions produced by ion irradiation on carbon nanotubes *Phys. Lett.* A **324** 321–5
[17] Ishaq A, Ni Z C, Yan L, Gong J L and Zhu D Z 2010 Constructing carbon nanotube junctions by Ar ion beam irradiation *Radiat. Phys. Chem.* **79** 687–91
[18] Kaikanov M, Amanzhulov B, Demeuova G, Akhtanova G, Bozheyev F, Kemelbay A and Tikhonov A 2020 Modification of silver nanowire coatings with intense pulsed ion beam for transparent heaters *Nanomaterials* **10** 2153
[19] Garnett E C, Cai W S, Cha J J, Mahmood F, Connor S T, Greyson Christoforo M, Cui Y, McGehee M D and Brongersma M L 2012 Self-limited plasmonic welding of silver nanowire junctions *Nat. Mater.* **11** 241–9
[20] Lin L C, Liu L, Musselman K, Zou G S, Duley W W and Zhou Y N 2016 Plasmonic-radiation-enhanced metal oxide nanowire heterojunctions for controllable multilevel memory *Adv. Funct. Mater.* **26** 5979–86
[21] Thamaraiselvan C, Wang J B, James D K, Narkhede P, Singh S P, Jassby D, Tour J M and Arnusch C J 2020 Laser-induced graphene and carbon nanotubes as conductive carbon-based materials in environmental technology *Mater. Today* **34** 115–31